Integrated coherent beam combining system for orbital-angular-momentum shift Keying based free-space optical links

Bowang Shu,[a] Yuqiu Zhang,[a,*] Hongxiang Chang,[a] Shiqing Tang,[a] Jinyong Leng,[a,b,c] and Pu Zhou[a,*]
[a] National University of Defense Technology, College of Advanced Interdisciplinary Studies, Changsha, China
[b] National University of Defense Technology, Nanhu Laser Laboratory, Changsha, China
[c] National University of Defense Technology, Hunan Provincial Key Laboratory of High Energy Laser Technology, Changsha, China

Abstract. Orbital-angular-momentum (OAM) multiplexing technology offers a significant dimension to enlarge communication capacity in free-space optical links. The coherent beam combining (CBC) system can simultaneously realize OAM multiplexing and achieve high power laser output, providing substantial advantages for long-distance communication. Herein, we present an integrated CBC system for free-space optical links based on OAM multiplexing and demultiplexing technologies for the first time. A novel method to achieve flexible OAM multiplexing and efficient demultiplexing based on CBC system is proposed and demonstrated both theoretically and experimentally. The experimental results exhibit a low bit error rate (BER) of 0.47 % and high recognition precision of 98.58 % throughout the entire data transmission process. By employing such ingenious strategy, this work holds promising prospects for enriching ultra-long distance structured light communication in the future.

Keywords: Orbital-angular-momentum, coherent beam combining, free-space optical communication, bit error rate.

***Sixth Author, E-mail: zhoupu203@163.com, *Second Author, E-mail: zhangyq914@163.com**

1 Introduction

Since optical vortices carrying orbital-angular-momentum (OAM) was proved by L. Allen in 1992[1], it has aroused great interest in the study of structured light. Due to the novel properties of OAM modes, such as orthogonality between different modes and infinite topological charges, it provides potential application prospect for free-space optical communication (FSOC)[2, 3]. Exceeding the capabilities of traditional multiplexing, such as time, wavelengths, frequency and polarization[4, 5], OAM modes possesses the potential to provide a new degree of freedom for multiplexing data transmission.

Since 2004, Gibson firstly applied vortex beams into FSOC[6], this finding arouses much research in OAM shift keying based free-space optical links[7-9]. Then, the performances of FSOC system on the basis of OAM multiplexing technology are greatly improved when combined with space division multiplexing[10, 11], wavelength division multiplexing, quadrature amplitude modulation technology and so on. Correspondingly, OAM mode demultiplexing has been developed, such as direct measurement, interferometry, diffraction measurement and deep learning[12-14]. In 2012, Wang et al. achieved OAM multiplexed data transmission with large capacity of 2.56 Tb per second (Tb/s) [15]. Then, Willner A.E. realized data transmission at the speed of 100 Tb/s one year later[16]. Up to now, the capacity of structured light communication achieved the highest value equaling 1.036 Pb per second (Pb/s)[17].

During long-term development, the scope of application has been gradually enlarged, especially, the demand for transmission distance have been higher than before. As Prof. Djordjevic has proved that the frequency spectrum efficiency of communication can be improved significantly by OAM modes modulation in near-earth and deep space[18], it provides new insight into communication range, which could further expand to earth-star, star-star and even deep space. However, the problems of atmospheric turbulence[19] and divergence of OAM beams[20] may cause power loss, that is, limitation in crucial device affect transmission distance and stability is still challenging.

In order to satisfy ultra-long communication distance and highly integrated system, coherent beam combining (CBC) system could be a good solution to solve above problems[21]. In 2020, Tales Research Center built a 61-channel fiber laser array system and generated femtosecond vortex beams with 800 W output power[22]. In 2023, Long et al. reported that 1.5 kW fractional vortex beam has been obtained by CBC[23]. These results illustrated CBC system possessed the potential in generation of high-power structured light. Previously, Hou et al. analyzed the corresponding characteristics of synthesized vortex beams including mode purity and OAM spectra, which indicated that OAM beams could be well controlled by coherent laser array (CBA)[24]. Although large quantity OAM modes are faced with mode crosstalk and dispersion as to be multiplexed together[25], the independent and distributed sub-apertures of CBA is enough to support superposition of large amount of OAM modes. Recently, the transmission of telecom signal has been successfully realized by CBC system[26, 27], and the atmospheric turbulence effects on the performance of OAM multiplexed optical links have been studied theoretically under the structure of CBA[28]. Thus, CBC system could play an important role in realizing structured light communication.

Herein, we have designed an integrated CBC system for the first time, which is divided into three parts of OAM mode multiplexing, filtering and propagation and OAM mode demultiplexing. The system is not only able to flexibly generate multiplexing optical vortices by several ring-shaped sub-arrays, but also precisely realize reliable detection by complex forking gratings both theoretically and experimentally. Based on the efficient decoupling method, the system ensured data transmission with a low bit error rate (BER) of 0.47 % and a high recognition precision of 98.58 %. Hopefully, CBC system is expected to be a good solution in ultra-long and large-capacity transmission in the field of OAM shift keying based free-space optical links.

1.1 Working principles

Figure 1 illustrates the principles of structured optical communication by a CBA. As shown in Fig.1, the system is divided into three parts including OAM mode multiplexing (Mux), Filtering and Propagation, and OAM mode demultiplexing (Demux). The main role of Mux is to encode data into OAM superposition modes by a series of sub-arrays, and the number of sub-arrays decides the number of communication channels. Then, the part of Filtering and Propagation is responsibility of transmitting assigned information in the form of vortex vortices, which is accompanied by spatial filtering. Lastly, the important role of Demux takes the job of receiving and analyzing signals with the method of complex forking gratings, and the decoupling results are located in specific locations for convenience.

Considering a circularly arranged CBA is constructed by *M*-layer sub-arrays, and a bit data is encoded into each sub-array by the designed specific topological charge. Total incident light field is formed by *N* sub-apertures, and then split into *M* layers. The incident light field of CBA can be described as:

$$\begin{aligned} E(x_1,y_1) &= \sum_{j=1}^{N_1} A_0 T \exp[-\frac{(x_1-a_{1,j})^2+(y_1-b_{1,j})^2}{{w_0}^2}]\times\exp(\mathrm{i}l_1\varphi_{1,j}) \\ &+\sum_{j=1}^{N_2} A_0 T \exp[-\frac{(x_1-a_{2,j})^2+(y_1-b_{2,j})^2}{{w_0}^2}]\times\exp(\mathrm{i}l_2\varphi_{2,j}) \\ &+\ldots+\sum_{j=1}^{N_i} A_0 T \exp[-\frac{(x_1-a_{n,j})^2+(y_1-b_{n,j})^2}{{w_0}^2}]\times\exp(\mathrm{i}l_m\varphi_{m,j}) \\ &=\sum_{i=1}^{M}\sum_{j=1}^{N} A_0 T \exp[-\frac{(x_1-a_{i,j})^2+(y_1-b_{i,j})^2}{{w_0}^2}]\times\exp(\mathrm{i}l_i\varphi_{i,j}) \end{aligned}, \tag{1}$$

where (x_1 , y_1) is coordinates in the incident plane, and w_0 is the effective mode field radius of each Gaussian-shaped beamlet. Then, ($a_{i,j}$, $b_{i,j}$) is the central coordinate of the *j*-th channel beam in the *i*-th layer sub-array, where $a_{i,j}=R_i\cos\left[\frac{2\pi(j-1)}{N}\right]$ and $b_{i,j}=R_i\sin\left[\frac{2\pi(j-1)}{N}\right]$, respectively. Next, $N_i=6i$ is the total number of the *i*-th sub-array, and R_i is the distance between *i*-th layer and original point. $\varphi_{i,j}$ is the piston phase of the *j*-th channel Gaussian-shaped beam in the *i*-th sub-array, where $\varphi_{i,j}=\frac{2\pi l_i(j-1)}{N_i}$. l_i in Eq. (1) is the assigned topological charge in the *i*-th sub-array, and $l_1,l_2,\cdots,l_n$ should be unequal with each other to meet requirement of coherently combined OAM modes. Meanwhile, *T* is the circ function, which can be expressed to be:

$$T=circ[\frac{\sqrt{(x_1-a_{i,j})^2+(y_1-b_{i,j})^2}}{d/2}], \tag{2}$$

where *d* in Eq. (2) is size of apertures.

As shown in Fig. 1(a), we choose four sub-arrays (i = 2, 5, 8, 11) consisting of 12, 30, 48 and 66 sub-apertures to form CBA in near-field. The topological charges are set to be 1, 3, 5 and 7 from the internal layer to the external layer, respectively. As the single circular shaped sub-array has been proved to generate vortex beams successfully[29, 30], more sub-arrays could contribute to more multiplexed OAM modes.

Before arriving at the receiving terminal, the formed far-field pattern would go through a period of free-space propagation. During the process, spatial filtering system should be set in consideration of extra sidelobes seen in Fig. 1(b). Then, the results can be represented to be:

$$E(x_2, y_2) \approx \frac{\exp(i4\pi f_1 / \lambda)}{if_1\lambda} \mathrm{F}\{E(x_1, y_1)\}\, circ(\sqrt{x_2^{\,2} + y_2^{\,2}} / d_f) \,, \tag{3}$$

where (x_2 , y_2)is coordinates in the confocal plane, and $\mathrm{F}\{E(x_1, y_1)\}$ is Fourier transform of beamlets in the near-field. Then, f_1 in Eq. (3) is the focal length of lens in the 4f spatial filtering system, and d_f is the size of pinhole.

In the last part, these multiplexed OAM modes will be decoupled by diffraction gratings, and the corresponding expression of demultiplexing results can be written as:

$$E(x_3, y_3) \approx \frac{\exp(i4\pi f_2 / \lambda)}{if_2\lambda} \mathrm{F}\{E(x_2, y_2)\} \exp[i\phi_{grating}] \,, \tag{4}$$

where (x_3 , y_3) is coordinates in the far-field, and f_2 in Eq. (4) is the focal distance of lens in behind of space filtering system. Then, $\phi_{grating}$ in Eq. (5) can be described as:

$$\begin{aligned} \phi_{grating} &= \arg[\exp(i\frac{2\pi}{\lambda} x_3 \sin\eta_1 + i\frac{2\pi}{\lambda} y_3 \sin\xi_1 + il_1\varphi) \\ &\quad + \exp(i\frac{2\pi}{\lambda} x_3 \sin\eta_2 + i\frac{2\pi}{\lambda} y_3 \sin\xi_2 + il_2\varphi) \\ &\quad + ... + \exp(i\frac{2\pi}{\lambda} x_3 \sin\eta_3 + i\frac{2\pi}{\lambda} y_3 \sin\xi_3 + il_m\varphi)] \\ &= \arg[\sum_{i=1}^{m} \exp(i\frac{2\pi}{\lambda} x_3 \sin\eta_i + i\frac{2\pi}{\lambda} y_3 \sin\xi_i + il_i\varphi)] \end{aligned} \,, \tag{5}$$

(5)[10]

where φ is the azimuthal coordinate. From the above formula, it could be found that the diffraction grating is a kind of complex forking gratings, and each forking grating is the superposition of spiral phase and blazed grating phase. Hence, this method provides main function of decoupling different OAM modes towards different directions (η_i, ξ_i). When four sub-arrays are used in the transmitting terminal, the number of available OAM modes in the receiving terminal is four, that is, the diffraction grating is composed of four forking gratings as illustrated in Fig. 3(c).

The detected light intensity pattern in the far-field is expressed to be:

$$I = E(x_3, y_3) \times E(x_3, y_3)^* , \tag{6}$$

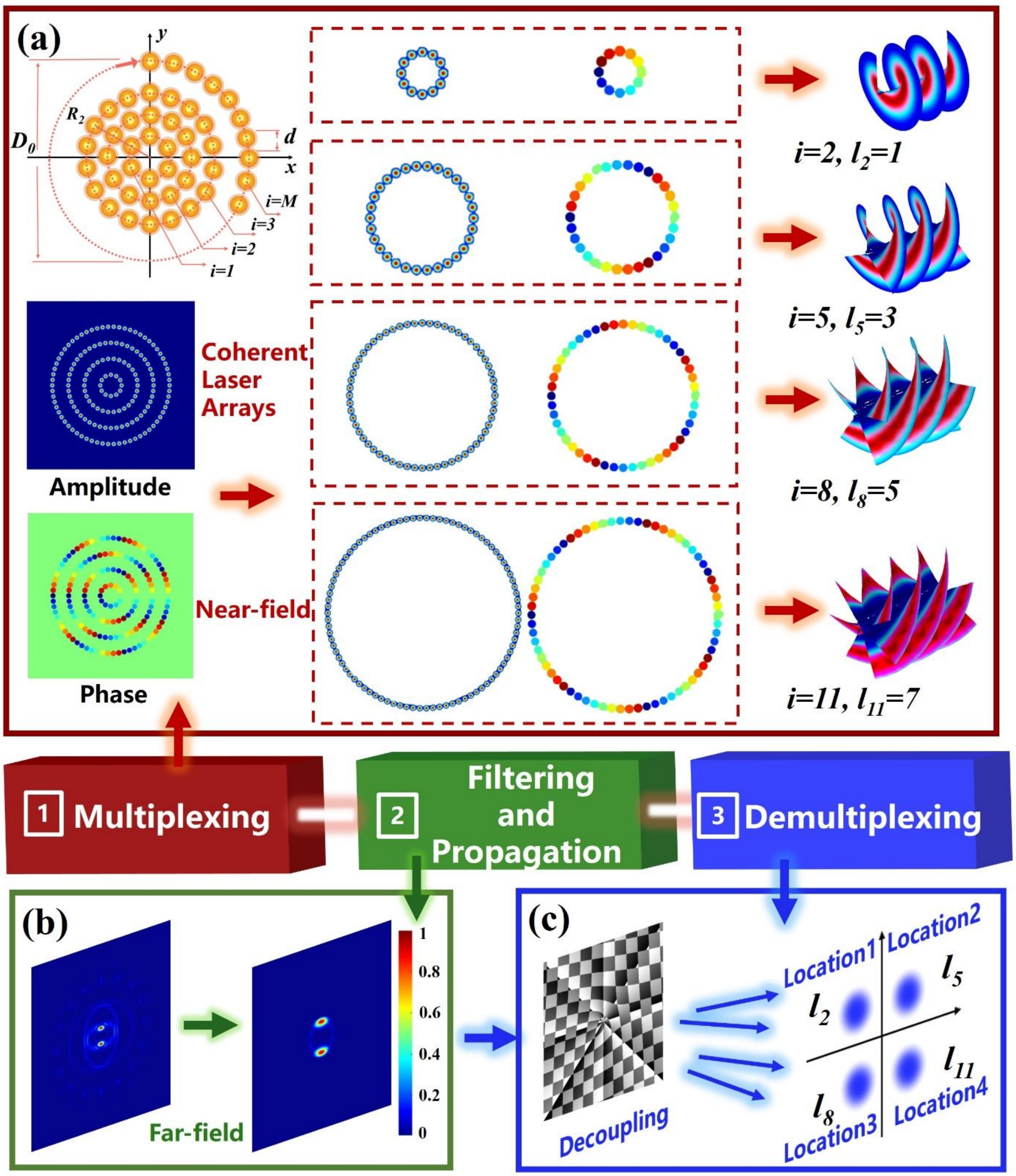

Fig. 1 Principles of structured optical communication by CBA. (a) The first part: Distributed tiled apertures in the near-field for generation of multiplexed optical vortices. (b) The second part: Filtering and Propagation process of the multiplexed OAM modes. (c) The last part: Demultiplexing of OAM modes by the designed diffraction grating.

1.2 Experimental set-up

The designed equivalent experimental device effectively validates the feasibility of optical communication, as demonstrated in Fig. 2, thereby achieving the function of data transmission through a CBC system. Firstly, the laser emitting from the seed is directed through a collimator (CO), followed by a beam expander (BE), a half-wave plate (HWP) and polarizers (P). Subsequently, it reaches the section dedicated to OAM mode multiplexing. The combination of an amplitude-spatial light modulator (A-SLM) and a phase-spatial light modulator (P-SLM1) enables the implementation of this part, thereby achieving a CBC system that is practically equivalent. Next, spatial filtering is achieved through a $4f$ (f = 1 m) device in green frame during free-space propagation. Lastly, the diffraction grating will be loaded on P-SLM2, and it corresponds to the third part of OAM mode demultiplexing within the blue frame. With the above architecture, three main parts including OAM modes multiplexing, spatial filtering and propagation, and OAM mode demultiplexing are perfectly integrated into the system.

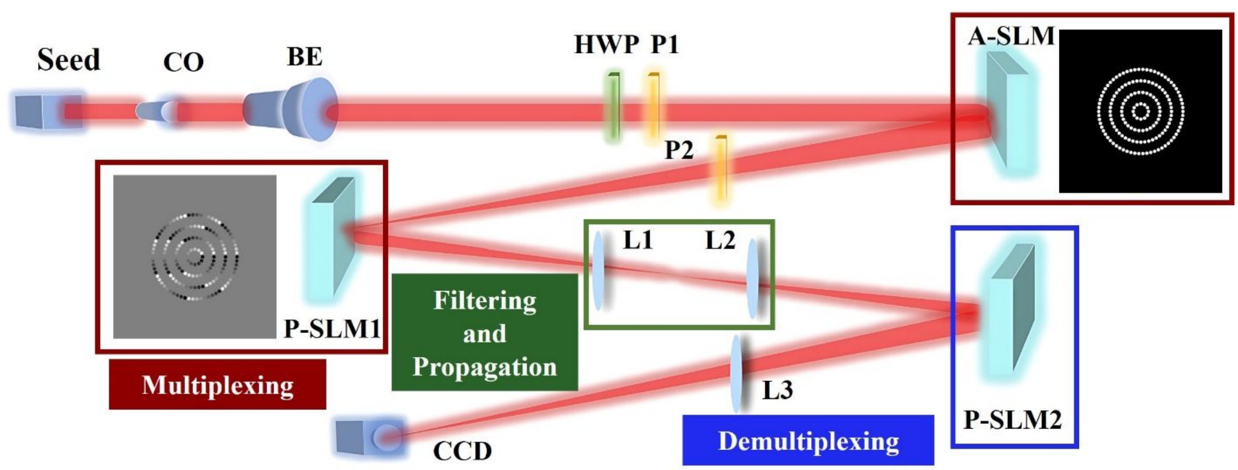

Fig. 2 The graphical diagram of CBA for FSOC system. The detailed components of experimental setup are CO: collimator, BE: beam expander, HWP: half-wave plate, P1-P2: polarizers, L1-L3: lenses, CCD: charge coupled devices, A-SLM: amplitude type spatial light modulator, P-SLM1 and P-SLM2: phase type spatial light modulators.

2 Results and Discussion

2.1 OAM modes multiplexing procedure by CBA

To validate the concept of OAM mode multiplexing, we amalgamate the second, fifth, eighth and eleventh sub-arrays together, while assigning them corresponding topological charges of 1, 3, 5 and 7, respectively. If we choose one, two, three or four of total sub-arrays at a time, there are totally fifteen possibilities of multiplexed OAM modes as shown in Fig. 3(a1) - (a15). Here, we label the layer of sub-array utilized in the patterns. For example, Fig. 3(a1) illustrates that only a single OAM mode is multiplexed by one sub-array (i=11), indicating the participation of a sole OAM mode. And Fig. 3(a6) illustrates two sub-arrays (i=5 and i=8) are employed to multiplex OAM modes, resulting in the formation of superposition states. At the condition of superposed two OAM modes, it could be observed that the number of petals in multiplexed OAM modes from far-field intensity pattern is $|l_1 - l_2|$. As three or more OAM modes are combined, these patterns exhibit two prominent intensity focus points that differ in size.

When the intensity and phase distribution are loaded on the A-SLM and P-SLM1, respectively, the experimental results exhibit a high degree of consistency with the corresponding theoretical patterns, as shown in Fig. 3(b1) - (b15). Thus, OAM modes multiplexing have been successfully realized with help of this strategy. Building upon above findings, it shows that the expansion of OAM mode multiplexing on a larger scale could be achieved by incorporating additional sub-arrays. In this paper, four sub-arrays fundamentally essentially fulfill the demands in the process of data transmission.

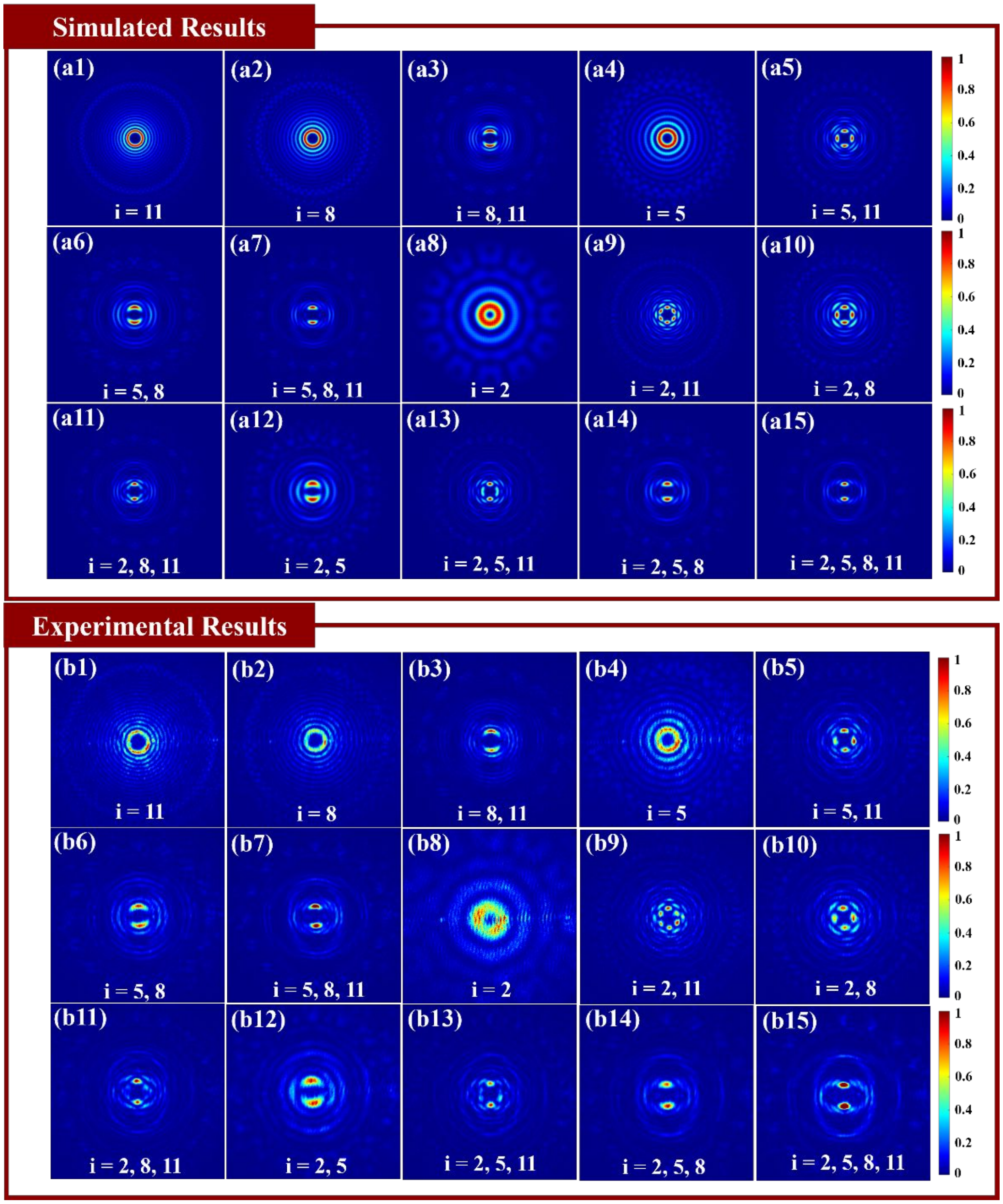

Fig. 3 The verification results of OAM mode multiplexing by CBA. (a1) - (a15) Simulated results of OAM mode multiplexing in the far-field. (b1) - (b15) Experimental results of OAM modes multiplexing in the far-field.

To further elucidate the underlying mechanism of OAM mode multiplexing by CBA, this section delves into more variables. As shown in Fig. 4(a1) - (a3), the emission source is mainly organized by two sub-arrays with opposite topological charge ($TC1 = -1$; $TC2 = 1$). Except intrinsic phase differences, extra phase differences of $\Delta\varphi = 5\pi/4, \pi, 5\pi/3$ are added between these two sub-arrays, respectively. As depicted in Fig. 4(b1) - (b3), the corresponding far-field pattens are differed only in rotation directions, which indicate that the initial phase distribution between different layers will not cause essential influences under different conditions. The experimental results further prove it in Fig. 4(c1) - (c3).

It is known that high-capacity FSOC system needs the participation of large amount of OAM modes, which implies the need for the generation of high-order OAM modes. As it is well-known, the maximum achievable topological charge can be set to be $l/3$[31]. To achieve high-order OAM modes, an increased number of sub-apertures within each sub-array could be utilized. The phase distribution in Fig. 4(d1) - (d3) exhibits distinct arrangements, with the CBA consisting of "12 (i=2) and 18 (i=3)" sub-apertures, "30 (i=5) and 36 (i=6)" sub-apertures, as well as "48 (i=8) and 54 (i=9)" sub-apertures. Accordingly, the topological charge is set to be "-2 and 3" from the internal layer to the external layer, respectively. On one hand, it can be found that the number of sub-apertures does not affect intensity distribution as shown in Fig. 4(e1) - (e3). On the other hand, a greater number of sub-apertures in a single sub-array simultaneously enables satisfaction of high-order OAM modes. This observation is further proved by experimental results as shown in Fig. 4(f1) - (f3).

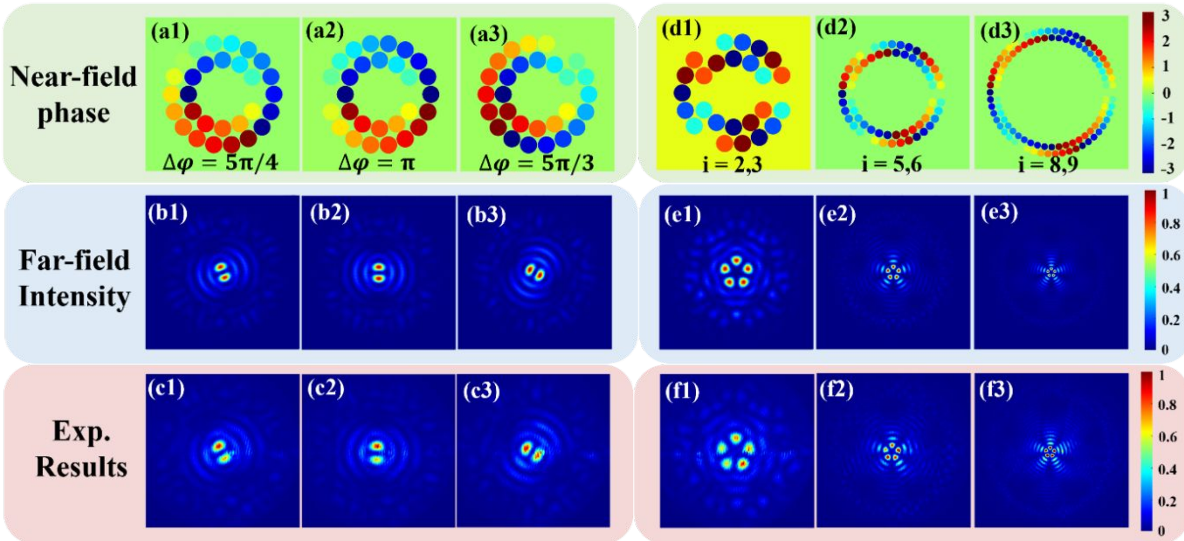

Fig. 4 The intensity and phase distribution of OAM modes multiplexing by two sub-arrays with phase differences or with different sub-apertures. (a1) - (a3) Near-field phase distribution of two sub-arrays with phase differences. (b1) - (b3) Simulated results of multiplexed OAM modes by two sub-arrays with phase differences. (c1) - (c3) Corresponding experimental results. (d1) - (d3) Near-field phase distribution of two sub-arrays with different sub-apertures. (e1) - (e3) Simulated results of multiplexed OAM modes by two sub-arrays with different sub-apertures. (f1) - (f3) Corresponding experimental results.

2.2 Filtering and propagation procedure

The presence of sidelobes in the far-field resulting from CBC technology is a commonly observed phenomenon. According to Hou et. al investigations, the mode information of OAM beams mainly existing in the central spots and surrounding sidelobes are formed by the interferences of high-order OAM modes in CBC system[24]. To achieve precise results of Demux technique, it is essential to incorporate spatial filtering into the free-space propagation procedure. Spatial filtering plays a crucial role in improving the accuracy and reliability of Demux technique by effectively removing unwanted interference or noise from the intensity signals. This process involves applying mathematical algorithms that exploit the spatial characteristics of the signals to separate them effectively. Then, the filtered signals can be analyzed or utilized for various applications such as communication systems, imaging technologies, or scientific research. The far-field patterns are illustrated in Fig. 5(a1) - (a15). Compared with Fig. 5(b1) - (b15), it is demonstrated that the experimental results exhibit a high level of concordance with the theoretical results. The spatial technology effectively eliminates the sidelobes, ensuring a prominent main lobe. In practical, the limited ability of spatial filtering could lead to some residual sidelobes in the experimental results. However, the proposed decoupling method exhibits robustness to tolerate this phenomenon.

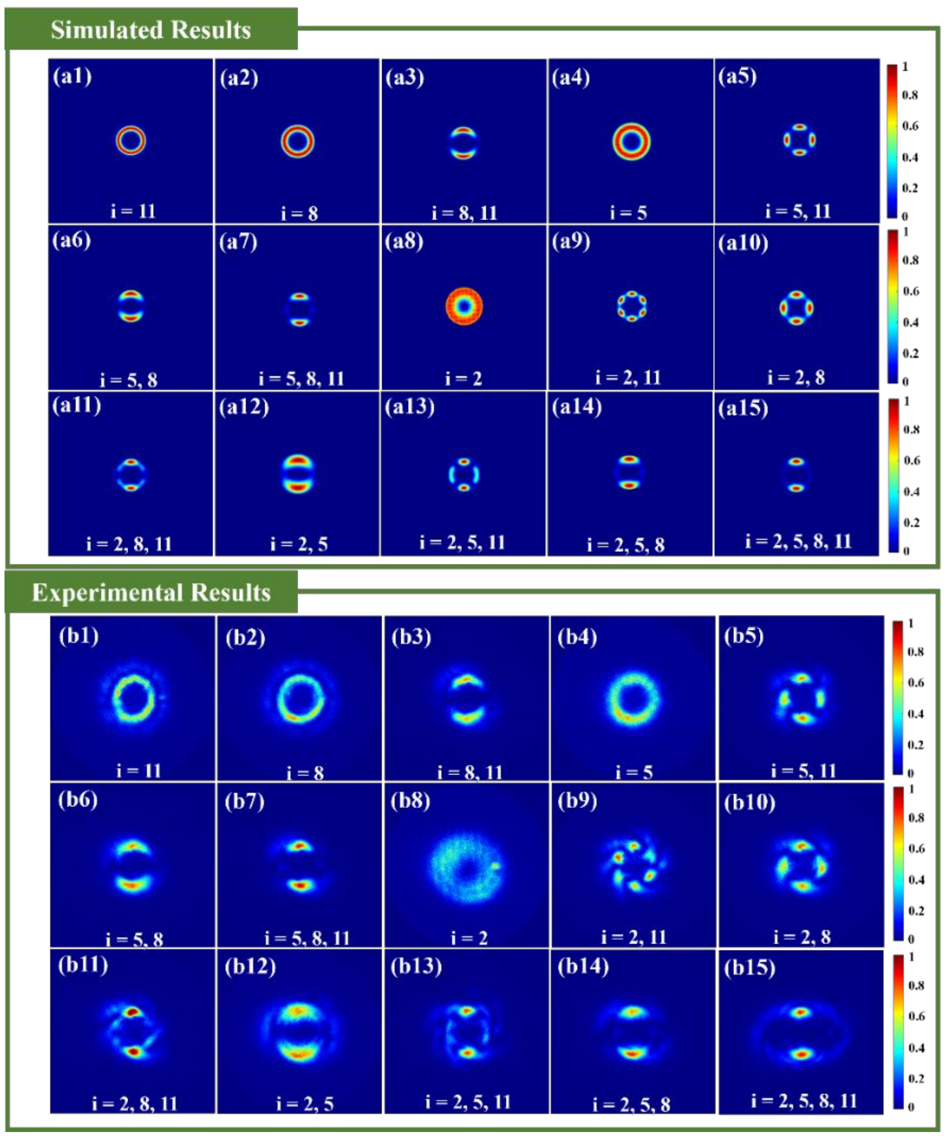

Fig. 5 The intensity distribution in the far-field by spatial filtering between multiplexing and demultiplexing procedure. (a1) - (a15) Simulated results. (b1) - (b15) Corresponding experimental results.

2.3 OAM modes demultiplexing procedure by complex forking gratings

Diffraction grating as decoupling strategy is commonly to be utilized for analysis of OAM mode information. In this work, the complex forking grating is chosen as the diffraction grating in the integrated CBC system, possessing a binary function. The first aspect involves the demultiplexing of four specific OAM modes, each possessing topological charges of 1, 3, 5 and 7. The second aspect pertains to the spatial separation of these four OAM modes into designed locations at -45°, 45°, -135° and 135° angles denoted as Location 1 to 4 as shown in Fig. 1(c). It is due to each forking grating is the superposition of spiral phase and blazed grating phase. Surely, the coordination in each location can be changed by blazed gratings phase according to its parameters, and the demultiplexed OAM modes are decided by spiral phase according to topological charges of participated OAM modes.

The appearance of a Gaussian spot at on Location after passing through the complex forking gratings indicates the presence of the corresponding OAM mode component. For example, if the OAM mode (l_2=1) goes through free-space propagation, the Gaussian point will appear at the Location 1 as shown in Fig. 6(a9). If both two OAM modes (l_2=1 and l_8=5) go through free-space propagation, the Gaussian point will appear at the Location 1 and Location 3 simultaneously as depicted in Fig. 6(a10). Theoretically, by employing the efficient decoupling methods, it could precisely judge the existing OAM modes in patterns by white circles in Fig. 6(a1) - (a15). The experimental results are shown in Fig. 6(b1) - (b15), and the detected results could be finely to be recognized. If none sub-array added, there are sixteen results of OAM mode multiplexing in total. These sixteen far-field patterns formed by specific groups of sub-arrays could be utilized to encode, which means it can transmit multiple information by loading on the far-field light field.

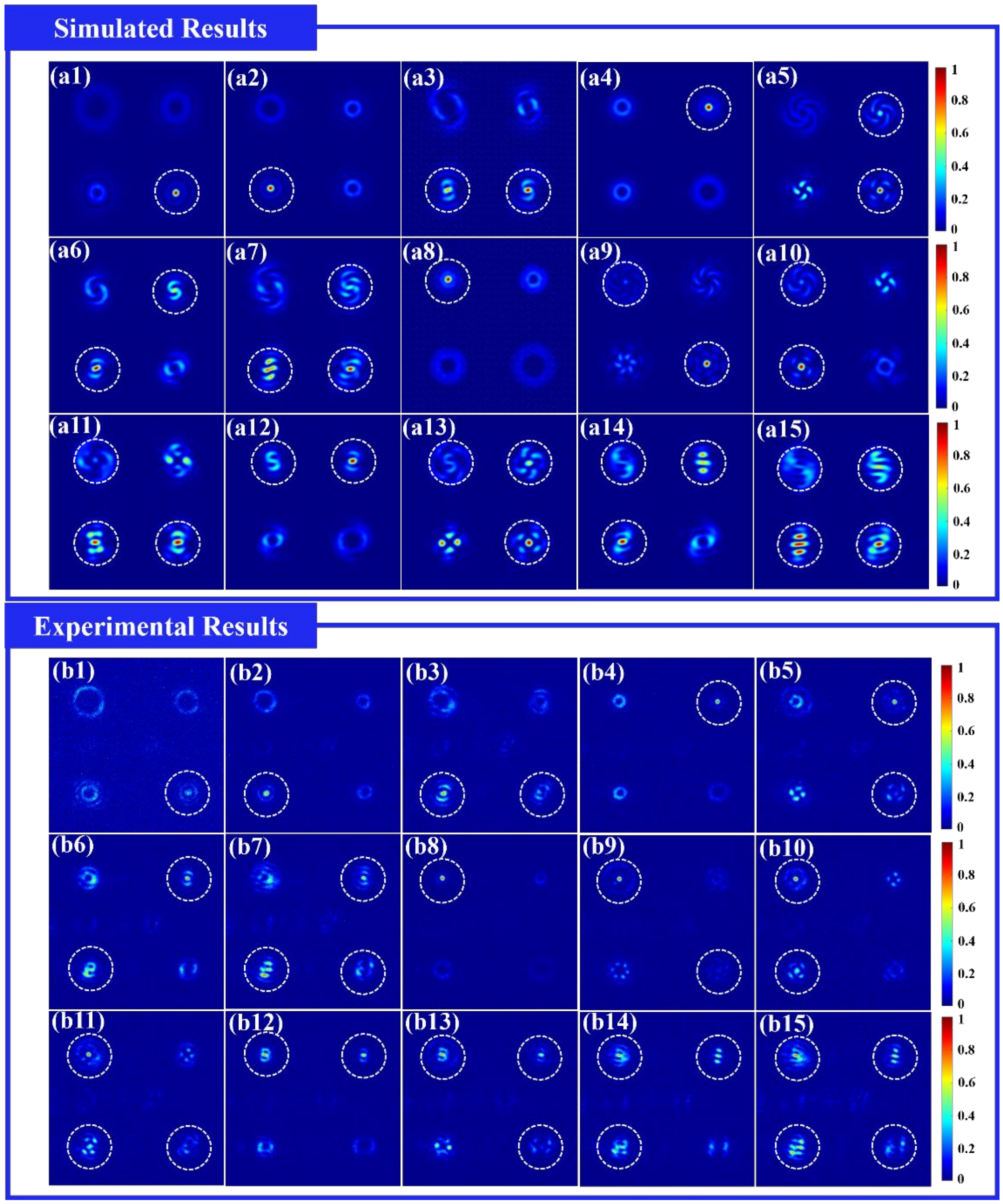

Fig. 6 The verification results of OAM mode demultiplexing by complex forking gratings. (a1) - (a15) Simulated results of OAM mode multiplexing in the far-field. (b1) - (b15) Experimental results of OAM mode multiplexing in the far-field.

The field intensities overlap between the simulated and experimental results could be represented by correlation, which is defined to be: $C=\left|\frac{\iint \Delta I_t(r,\varphi)\Delta I_e(r,\varphi) r\mathrm{d}r\mathrm{d}\varphi}{\sqrt{\iint \Delta I_t^2(r,\varphi) r\mathrm{d}r\mathrm{d}\varphi \iint \Delta I_e^2(r,\varphi) r\mathrm{d}r\mathrm{d}\varphi}}\right|$, where $\Delta I_k(r,\varphi)=I_k(r,\varphi)-\overline{I}_k(r,\varphi)(k=t,e)$, and the correlation value is within the range of 0-1. In the above expression, $\overline{I}_k$ represents the corresponding mean value of theoretical far-field intensity I_t or I_e. On the basis of calculated results, the correlation values between the simulated and experimental results in Fig. 3 and Fig.5 are within the range of 0.85 - 0.95, which means the simulated results of far-field light distribution match well with corresponding experimental results regardless of spatial filtering. However, the correlation value in Fig. 6 decrease to be around 0.5. The reason for this phenomenon is that the unstable factors in experimental equipment. It is most probably that the offset of light spots in path, which result in the failure alignment between the experimental and calculated decoupling results. To note that, the whole decoupling process is only influenced by the intensity in the central Gaussian points, so the correlation values have no relationships with the recognition accuracy.

To note that, the phase coincidence is hard to meet in a practical CBC system. Herein, we further consider how the existence of phase errors affect the demultiplexing process. As shown in Fig. 7, we select several specific codes including '0001', '1010', '1110' and '1111' for comparison as the added phase errors (σ_p^2) to be 0, 0.3, 0.6, 1.0 and 1.5, respectively. These four codes are varied by different numbers of multiplexed OAM modes that required to be recognized. Obviously, if phase errors are introduced in the whole system, it will affect the precision of demultiplexing results to some extent. When the introduced phase errors are below 1.0, most of the codes could be precisely identified. Once exceeding the value, the error rate will significantly increase, even disable up to be 1.5. for example, the error codes '1010' in Fig. 7(b4) – (b5), '1110' in Fig. 7(c4) – (c5) and '1111' in Fig. 7(d5) are not recognized correctly. In consideration of simplifying the system and ensuring the quality of communication links, we only perform data transmission in ideal scenario.

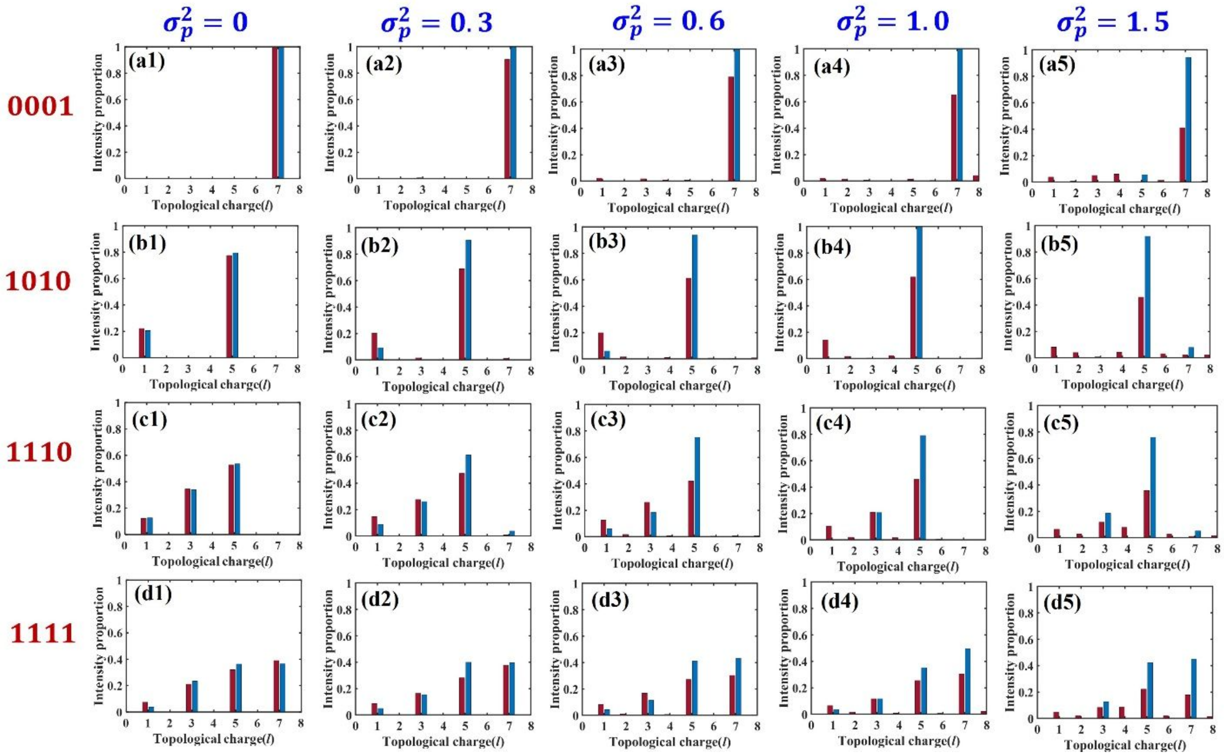

Fig. 7 The comparison between simulated intensity proportion of ideal OAM modes and practical OAM modes before and after demultiplexing process. Results of the codes to be (a1) - (a5) ‘0001’; (b1) - (b5) ‘1010’; (c1) - (c5) ‘1110’ and (d1) - (d5) ‘1111’ as introduced phase errors to be 0, 0.3, 0.6, 1.0 and 1.5, respectively.

2.4 Data transmission by integrated CBC system

By the proposed integrated CBC system, we successfully present transmission of the image called ‘Ke Xiaobo’ at a resolution of 25*50. Due to a single pixel consisted by 8 bits, the number of transmitting code element is 25*50*8 equaling 10000 totally. The detailed recognition process of single pixel is on the basis of image processing. For example, if a single pixel equaling 74 is chosen, which should be transferred to be binary coding ‘01001010’ firstly. These eight code elements are divided into two parts. The first four bits ‘0100’ could be loaded by the intensity and phase in Fig. 8(b1) - (c1), and the last four bits ‘1010’ could be loaded on the intensity and phase in Fig. 8(b2) - (c2). The multiplexing results are given in Fig. 8(d1) - (d2). After a period of filtering and free-space propagation, the obtained patterns are shown in Fig. 8(e1) - (e2). To realize automatic detection process, these two OAM demultiplexing results in Fig. 8(f1) - (f2) will be transferred into grayscale image in Fig. 8(g1) - (g2) for image processing. Next, we can define the existence or inexistence of mode to be 1 or 0. Four-bit binary coding can be realized by above four OAM modes, which means the data transmission can be further conducted. The corresponding encoding results '0100' and '1010' will be formed according to marked Gaussian light spots in Fig. 8(h1) - (h2). Lastly, the single pixel '74' is successfully coded. Based on above findings, these different OAM multiplexing results can support the encoding information from 0 to 15. If all pixels (0 ~ 255) in image of 'Ke Xiaobo' need to be expressed, the amount of far-field pattens is 25*50*2.

The error rate at different locations is shown in the Fig. 8(j), and the bar chart displays the error rate of four locations. It is demonstrated that the BER for the transmission of the image is 0.47 %, which corresponds to the ratio of incorrectly coded element to all coding element. It is obvious that the result falls within the range of 10^{-3}, meeting the requirements of a structured optical communication system. To note that, if the number of transmitting bits is large enough, then BER will decrease to some extent, which means it could be satisfy more requirements. Owing to the efficient and careful spatial filtering, the whole detection process is in high precision of 98.58 %. The presence of background noise and measurement instability leads to the identification of error code elements as depicted in Fig. 8.

During the transferring process of grayscale image, the setting of thresholds is the most crucial stage to confirm the existence of these four OAM modes. As can be seen in the Fig. 8(k1) - (k4), the four Gaussian spots in correspondence with each code have been separated into four regions, and the fixed area marked by red circles will be used for the settings of threshold. If the intensity value in such small region is higher than thresholds, the corresponding OAM mode will be detected, otherwise it will set to be zero. The method is similar to the grey-scale algorithms proposed by Fu et al[33]. As can be seen in the Fig. 8 (k5), the optimal performance of a structured optical communication system can be achieved by employing a perfect combination of the threshold in these four locations. We set the combination with lowest error rate to be standard, and the error rates become larger as the threshold difference increase. Thus. we finally verify the lowest BER to be 0.47 % after careful comparison between these different circumstances.

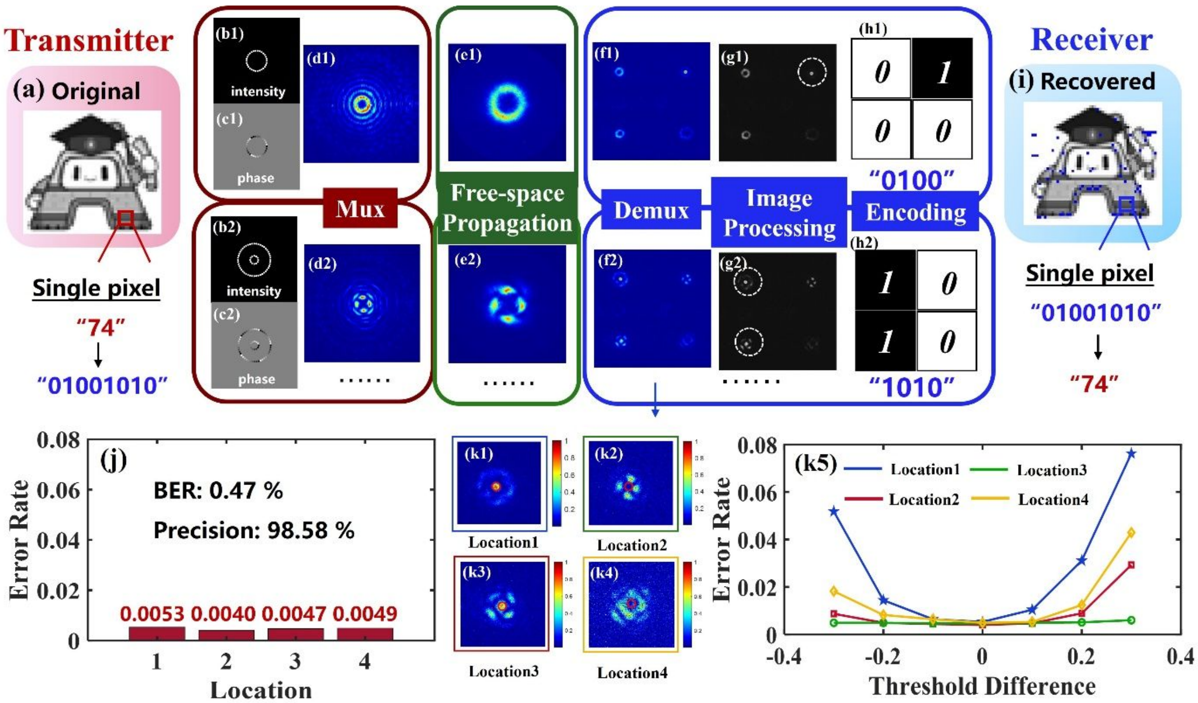

Fig. 8 The detailed process of data transmission by integrated CBC system. (a) Original input image. (b1) – (b2) Intensity, (c1) - (c2) phase distribution. (d1) - (d2) Far-field patterns, (e1) - (e2) Pattens after spatial filtering. (f1) - (f2) OAM modes demultiplexing results. (g1) - (g2) Transferred grayscale patterns. (h1) - (h2) The encoding results for '0100' and '1010' code elements, respectively. (i) Recovered output image. (j) Error rate at different locations. (k1) – (k4) The separate four Gaussian spots in consistent with Fig 8 (f2). (k5) Error rate at different thresholds.

3 Conclusion

To sum up, this work proposes an integrated CBC system for free-space structured optical communication. The system is divided into three parts including OAM mode multiplexing, filtering and propagation and OAM mode demultiplexing, respectively. Such designed system preliminarily verifies the possibilities of binary encoding data transmission by CBC technology, and it achieved impressive performances, for example, the BER is as low as 0.47 % and the recognition precision is as high as 98.58 %. Divergent-free or non-diffraction beams will be further developed to improve the transmission distances of optical links as supported by flexible beam shaping by coherent beam arrays. In addition, if larger-scale CBC system applied into optical links, more channels could be set to improve the efficiency of FSOC. Hopefully, FSOC with ultra-long communication distance and high-performance communication quality by such integrated CBC system possess great prospects in future.

Code, Data, and Materials Availability

The simulated and experimental data that support this work are available from the first authors on reasonable request.

Disclosures

The authors declare no competing financial interests.

Acknowledgments

This work is supported by National Natural Science Foundation of China under grant 62305388 and Postgraduate Scientific Research Innovation Project of Hunan Province under Grant QL20230007.

References

1. L. Allen et al., “Orbital angular momentum of light and the transformation of Laguerre-Gaussian laser modes,” *Phys. Rev. A* **45**(11), 8185-8189 (1992)
2. A. Forbes, M. de Oliveira, and M. R. Dennis, “Structured light,” *Nat. Photonics* **15**(4), 253-262 (2021)

3. A. E.Willner, “OAM Light for Communications,” *Opt. Photonics News* **32**(6), 34-41 (2021)
4. A. Yi et al., “Transmission of multi-dimensional signals for next generation optical communication systems,” *Opt. Commun.* **408**(9), 42-52 (2018)
5. N. Zhao et al., “Capacity limits of spatially multiplexed free-space communication,” *Nat. Photonics* **9**(12), 822-826 (2015)
6. G. Gibson et al., “Free-space information transfer using light beams carrying orbital angular momentum,” *Opt. Express* **12**(22): 5448-5456 (2004)
7. S. Fu et al., “Experimental demonstration of free-space multi-state orbital angular momentum shift keying,” *Opt. Lett.* **27**(23), 33111-33119 (2019)
8. S. Fu et al., “Demonstration of free-space one-to-many multicasting link from orbital angular momentum encoding,” *Opt. Lett.* **44**(19), 4753-4756 (2019)
9. Z. Shang et al., “Multiplexed vortex state array toward high-dimensional data multicasting,” *Opt. Express* **30**(19), 34053-34063 (2022)
10. Y. Awaji, N. Wada, and Y. Toda, “In Demonstration of spatial mode division multiplexing using Laguerre-Gaussian mode beam in telecom-wavelength,” in 23rd Annual Meeting of the IEEE Photonics Society, pp. 551-552, Denver, CO, USA (2010).
11. Y. Yan et al., “Multicasting in a spatial division multiplexing system based on optical orbital angular momentum,” *Opt. Lett.* **38**(19), 3930-3933 (2013)
12. S. Fu et al., “Simultaneous generation of multiple perfect polarization vortices with selective spatial states in various diffraction orders,” *Opt. Lett.* **41**(23), 5454-5457 (2016)
13. S. Li, and J. Wang, “Simultaneous demultiplexing and steering of multiple orbital angular momentum modes,” *Sci. Rep.* **5**, 15406 (2015)
14. Z. Liu et al., “Superhigh-Resolution Recognition of Optical Vortex Modes Assisted by a Deep-Learning Method,” *Phys. Rev. Lett.* **123**(18), 183902 (2019)
15. J. Wang et al., “Terabit free-space data transmission employing orbital angular momentum multiplexing,” *Nat. Photonics* **6**(7), 488-496 (2012)

16. H. Hao et al., “In 100 Tbit/s free-space data link using orbital angular momentum mode division multiplexing combined with wavelength division multiplexing,” in Optical Fiber Communication Conference and Exposition and the National Fiber Optic Engineers Conference (OFC/NFOEC), pp. 1-3, Anaheim, CA, USA (2013).
17. J. Wang et al., “In N-dimentional multiplexing link with 1.036-Pbit/s transmission capacity and 112.6-bit/s/Hz spectral efficiency using OFDM-8QAM signals over 368 WDM pol-muxed 26 OAM modes,” in European Conference on Optical Communication (ECOC), pp 1-3 (2014).
18. I. B. Djordjevic, “Deep-space and near-Earth optical communications by coded orbital angular momentum (OAM) modulation,” *Opt. Express* **19**(15), 14277-14289 (2011)
19. R. Zhang et al., “Simultaneous turbulence mitigation and channel demultiplexing for two 100 Gbit/s orbital-angular-momentum multiplexed beams by adaptive wavefront shaping and diffusing,” *Opt. Lett.* **45**(3), 702-705 (2020)
20. M. J. Padgett et al., “Divergence of an orbital-angular-momentum-carrying beam upon propagation,” *New J. Phys.* **17**(2), 023011 (2015)
21. D. Lin et al., “Reconfigurable structured light generation in a multicore fiber amplifier,” *Nat. Commun.* **11**(1), 1-9 (2020)
22. M. Veinhard et al., “Orbital angular momentum beams generation from 61 channels coherent beam combining femtosecond digital laser,” *Opt. Lett.* **46**(1), 25-28 (2021)
23. J. Long et al., “Generating the 1.5 kW mode-tunable fractional vortex beam by a coherent beam combining system,” *Opt. Lett.* **48**(19), 5021-5024 (2023)
24. T. Hou et al., “Higher-Order Airy Patterns and Their Application in Tailoring Orbital Angular Momentum Beams with Fiber Laser Arrays,” *J. Lightwave Technol.* **39**(14), 4758-4768 (2021)
25. J. A. Anguita, M. A. Neifeld, and B. V. Vasic, “Turbulence-induced channel crosstalk in an orbital angular momentum-multiplexed free-space optical link,” *Appl. Opt.* **47**(13), 2414-2429 (2008)
26. B. Rouzé et al., “Experimental study of the impact of carrying a telecom signal on LOCSET-based coherent beam combining,” *Opt. Express* **31**(16), 26552-26564 (2023)

27. V. Billault et al., “Optical coherent combining of high-power optical amplifiers for free-space optical communications,” *Opt. Lett.* **48**(14), 3649-3652 (2023)

28. P. Ju et al., “Atmospheric Turbulence Effects on the Performance of Orbital Angular Momentum Multiplexed Free-Space Optical Links Using Coherent Beam Combining,” *Photonics* **10**(6), 634 (2023)

29. Q. Sun et al., “Generating a Bessel-Gaussian beam for the application in optical engineering,” *Sci. Rep*. **5**(5), 18665 (2015)

30. H. Xia et al., “The generation and verification of Bessel-Gaussian beam based on coherent beam combining,” *Results Phys.* **16**, 102872 (2020)

31. V. P. Aksenov, V. V. Dudorov, and V. V. Kolosov, “Characterization of vortex beams synthesized on the basis of a fiber laser array,” in 21st International Symposium Atmospheric and Ocean Optics: Atmospheric Physics, *Proc. SPIE* **9680**, 96802D (2015).

32. Y An et al., “Learning to decompose the modes in few-mode fibers with deep convolutional neural network,” *Opt. Express* **27**, 10127 – 10137(2019).

33. S Fu et al.; “Measurement of orbital angular momentum spectra of multiplexing optical vortices,” *Opt. Express* **24**(6). 6240-6248(2016).

Pu Zhou is a professor at the National University of Defense Technology. He received his PhD degree in optical engineering from the National University of Defense Technology in 2009. He is the author of more than 100 journal papers. His current research interests include fiber laser technology, interdisciplinary field and so on.

Biographies and photographs for the other authors are not available.